Clim Dyn (2013) 41:2199–2212
DOI 10.1007/s00382-013-1934-2

Variability of the Indian Ocean SST and its possible impact on summer western North Pacific anticyclone in the NCEP Climate Forecast System

Xingwen Jiang · Song Yang · Jianping Li · Yueqing Li · Haoran Hu · Yi Lian

Received: 27 December 2012 / Accepted: 26 August 2013 / Published online: 3 September 2013

Abstract The NCEP Climate Forecast System version 2 (CFSv2) provides important source of information about the seasonal prediction of climate over the Indo-Pacific oceans. In this study, the authors provide a comprehensive assessment of the prediction of sea surface temperature (SST) in the tropical Indian Ocean (IO). They also investigate the impact of tropical IO SST on the summer anomalous anticyclonic circulation over the western North Pacific (WNPAC), focusing on the relative contributions of local SST and remote forcing of tropical IO SST to WNPAC variations. The CFSv2 captures the two most dominant modes of summer tropical IO SST: the IO basin warming (IOBW) mode and the IO dipole (IOD) mode, as well as their relationship with El Niño-Southern Oscillation (ENSO). However, it produces a cold SST bias in IO, which may be attributed to deeper-than-observed mixed layer and smaller-than-observed total downward heat flux in the tropical IO. It also overestimates the correlations of ENSO with IOBW and IOD, but underestimates the magnitude of IOD and summer IOBW. The CFSv2 captures the climate anomalies related to IOBW but not those related to IOD. It depicts the impact of summer IOBW on WNPAC via the equatorial Kelvin wave, which contributes to the maintenance of WNPAC in July and August. The WNPAC in June is mostly forced by local cold SST, which is better predicted by the CFSv2 compared to July and August. The mechanism for WNPAC maintenance may vary with lead time in the CFSv2.

Keywords Indian Ocean · Anticyclonic circulation over the western North Pacific · NCEP Climate Forecast System

This paper is a contribution to the Topical Collection on Climate Forecast System Version 2 (CFSv2). CFSv2 is a coupled global climate model and was implemented by National Centers for Environmental Prediction (NCEP) in seasonal forecasting operations in March 2011. This Topical Collection is coordinated by Jin Huang, Arun Kumar, Jim Kinter and Annarita Mariotti.

X. Jiang · Y. Li · H. Hu
Institute of Plateau Meteorology, China Meteorological Administration, Chengdu, Sichuan, China

S. Yang (✉)
Department of Atmospheric Sciences, Sun Yat-sen University, Guangzhou 510275, Guangdong, China
e-mail: yangsong3@mail.sysu.edu.cn

J. Li
National Key Laboratory of Atmospheric Sciences and Geophysical Fluid Dynamics, Institute of Atmospheric Physics, Chinese Academy of Sciences, Beijing, China

Y. Lian
Institute of Meteorological Sciences of Jilin Province, Changchun, Jilin, China

1 Introduction

The Indian Ocean (IO) sea surface temperature (SST) is significantly linked to the variability of local and remote climate (Fasullo and Webster 2002; Yoo et al. 2006; Xie et al. 2009; Ding et al. 2010; Li et al. 2010; Jiang and Li 2011; Yuan et al. 2012). The first two dominant modes of tropical IO SST are the IO basin-wide warming (IOBW) mode and the IO dipole (IOD) mode (Saji et al. 1999; Webster et al. 1999). Particularly, the summer IOBW is accompanied by anomalous anticyclonic circulation over the western North Pacific (WNPAC) during El Niño decaying summers, which affects the Mei-yu, Baiu, and Changma over East Asia by modulating the western Pacific subtropical high (WPSH; Chang et al. 2000; Li and Wang

2005; Lau and Wang 2006; Yoo et al. 2006; Xie et al. 2009, 2010; Chowdary et al. 2010, 2011; Huang et al. 2010; Wu et al. 2010; Zheng et al. 2011; Yuan et al. 2012). The WPSH and associated East Asian rainfall as well as the tropical storms over the subtropical western North Pacific (WNP) can be better predicted by a physically based empirical model compared to dynamical models (Wu et al. 2009; Wang et al. 2013). The IOD, which sometimes follows El Niño-Southern Oscillation (ENSO), plays a role of modulator for the Indian summer monsoon rainfall and affects the correlation between the monsoon rainfall and ENSO (Saji et al. 1999; Saji and Yamagata 2003; Ashok et al. 2001; Behera et al. 2005). It also has a decayed impact on the East Asia-western Pacific summer monsoon (Kripalani et al. 2010).

ENSO and related teleconnection patterns are the basis for the seasonal prediction in many regions (Shukla and Paolina 1983; Webster et al. 1998; Jiang et al. 2013a, b). Thus, the variability of tropical Pacific SST has received more attentions compared to the variability of IO SST. In spite of the success in ENSO prediction, there is also an apparent bias in predicting ENSO-related climate anomalies by dynamical models especially for those anomalies outside the tropical central and eastern Pacific (e.g. Jiang et al. 2013a, b). Previous studies have indicated that the IO is important for the relationship of ENSO with climate over the IO and the western Pacific (e.g. Yu and Lau 2004; Wu and Kirtman 2004a; Xie et al. 2009). Moreover, variations of the IO SST also exert a feedback on ENSO (e.g. Yu et al. 2002; Wu and Kirtman 2004b; Kug and Kang 2006; Yoo et al. 2010). Thus, there is an increasing interest in the predictability of IO and its climate impact. The predictability limit and forecast skill of tropical IO SST are generally lower than those of the tropical Pacific SST (e.g. Li and Ding 2012; Shi et al. 2012). The SST in the east and west portions of tropical IO can be predicted by 5–6 months and 6–9 months in advance, while the IOD can only be predicted by 3–4 months ahead (e.g. Shi et al. 2012). However, the impact of tropical IOBW on western North Pacific climate during El Niño decaying summer can be well predicted by some coupled ocean–atmosphere models (Chowdary et al. 2010).

The National Centers for Environmental Prediction (NCEP) Climate Forecast System (CFS), a fully-coupled forecast system, provides operational prediction of the world climate (Saha et al. 2006). Previous studies have reported that the CFS version 1 (CFSv1) has an apparent bias in predicting IO SST, which may limit the prediction skill of Asian summer monsoon (Yang et al. 2008; Pokhrel et al. 2012). In March 2011, a new version of the CFS, CFS version 2 (CFSv2), replaced the CFSv1. Compared to CFSv1, the CFSv2 incorporates a number of new physical packages for cloud-aerosol-radiation, land surface, ocean and sea ice processes, and a new atmosphere–ocean–land data assimilation system (Saha et al. 2010). Previous studies (e.g. Yuan et al. 2011; Jiang et al. 2013a) have shown increased skill in predicting global land precipitation and surface air temperature, as well as large-scale Asian summer monsoon, from CFSv1 to CFSv2. The CFSv2 also shows higher skill in predicting IOD (Shi et al. 2012) compared to the CFSv1. In spite of these advances, the CFSv2 is worse in predicting the South Asian (or Indian) summer monsoon compared to the CFSv1. Like CFSv1, the CFSv2 has apparent biases in predicting the Asian summer monsoon, with an exaggerated strong link of the monsoon to ENSO, for example (Jiang et al. 2013a). Given the important role of IO SST in the Indo-western Pacific climate, it is necessary to access how well the IO SST and its climate impact are predicted by the CFSv2.

Typically, the WNPAC forms during the fall of El Niño development years, reaches maximum intensity after El Niño matures, and persists through the following spring and summer (Wang et al. 2003). From the El Niño mature winter to the subsequent spring, the maintenance of the WNPAC is mainly attributed to a positive thermodynamic air-sea feedback (Wang et al. 2000). However, during El Niño decaying summer, it is ascribed to the remote forcing of IOBW (Xie et al. 2009) although the local atmosphere–ocean positive feedback may also prolong the El Nino's impact during this ENSO decaying phase (Wu et al. 2010; Wang et al. 2013). Using an atmospheric general circulation model (AGCM), Wu et al. (2010) reported that the maintenance mechanisms for the WNPAC during El Niño decaying summer varied from June to July. The contribution of local forcing of the negative SST anomalies (SSTA) in the WNP gradually weakens from June to August, while the contribution of remote forcing of IOBW gradually enhances (Wu et al. 2010). However, this result has been obtained from an AGCM simulation, which cannot realistically depict the air-sea interaction and may have bias in predicting the climate over the WNP (Wang et al. 2005; Jiang et al. 2013a). In addition, sensitive experiments conducted by Xie et al. (2009) indicate that the response of WNPAC to the forcing of IOBW is weak in an AGCM. Thus, it is important to investigate the relative contributions of the remote forcing of IOBW and the local forcing of cold SSTA to the maintenance of the WNPAC from June to August in an ocean–atmosphere coupled climate model.

The rest of this paper is organized as follows. Descriptions of the CFSv2 hindcast and observations used to verify CFSv2 output are given in Sect. 2. Prediction of IO SST by the CFSv2 is provided in Sect. 3. In Sect. 4, we investigate the prediction of the impact of IOBW on the WNPAC for summer mean, June, July, and August, respectively. A summary and further discussion of the results obtained are provided in Sect. 5.

2 Model, data and methods

The NCEP CFSv2 is a fully coupled dynamical prediction system (Saha et al. 2010). It consists of the NCEP Global Forecast System at T126 resolution, the Geophysical Fluid Dynamics Laboratory Modular Ocean Model versions 4.0 at 0.25°–0.5° grid spacing coupled with a two-layer sea ice model, and the four-layer Noah land surface model.

Output from the CFSv2 9-month hindcast is analyzed over a 28-year period of 1983–2010. Beginning on 1 January, 9-month hindcast runs were initialized from every 5th day and run from all 4 cycles of that day. The initial days vary from one month to another. A detail about the initial time can be found at http://cfs.ncep.noaa.gov/cfsv2.info/ (see file "Retrospective CFSv2 Forecast Data Information"). An ensemble seasonal mean of the monthly-mean values of 24 members is used, with initial dates after the 7th of the particular month used as the ensemble member for the next month. For JJA 0-month lead forecast, the ensemble mean of the runs initialized from 5 June and 11, 16, 21, 26, and 31 May is used as the forecast. The longest 7-month lead forecast for JJA is an ensemble mean of the runs initialized from 2 and 7 November and 8, 13, 18, 23, and 28 October. Beside the seasonal forecast, monthly mean forecast is also analyzed in this study. The ensemble members of monthly forecast are the same as those of seasonal forecast, but the longest lead of monthly mean forecast is 9 months. For example, 0-month lead forecast for June is the ensemble mean of runs initialized from 5 June and 11, 16, 21, 26, and 31 May, and the longest 9-month lead forecast is the ensemble mean of runs initialized from 3 September and 9, 14, 19, 24, and 29 August of the previous year.

The observations used for model verification include the Climate Prediction Center Merged Analysis of Precipitation (CMAP) (Xie and Arkin 1997), the winds, temperature, ocean mixed layer depth, and total downward heat flux at the sea surface from the NCEP Climate Forecast System Reanalysis (CFSR; Saha et al. 2010), and the SST from the NOAA OISST analysis (Reynolds et al. 2007). With first guess from a coupled atmosphere–ocean–sea ice–land forecast system, the CFSR has improved the climatological precipitation distribution over various regions and the interannual precipitation correlation with observations over the IO, the Maritime Continent, and the western Pacific compared to several previous reanalyses (Wang et al. 2010).

In this study, the Niño3.4 index is defined by the SST anomalies (SSTA) averaged over the Niño3.4 region (5°S–5°N, 120°–170°W). The IOD index is defined as the SSTA difference between the western (10°S–10°N, 50°–70°E) and the eastern (10°S–0°, 90°–110°E) tropical IO (Saji et al. 1999). We also define an IOBW index as the SSTA averaged within 20°S–20°N, 40°–110°E to describe the basin-wide SST mode over the tropical IO. We denote the ENSO developing year as year 0 and the following year as year 1. Thus, the summer [June–August (JJA)] of the ENSO developing year is symbolized as JJA(0), while the summer of the following years as JJA(1).

3 Prediction of IO SST

3.1 0-month lead prediction

Figure 1 shows the JJA mean SST and 850-hPa winds in 0-month lead hindcast and observation, along with their differences. The Indo-western Pacific is featured by warm SST in summer, which exceeds 28 °C in most of the region. The summer monsoon flow has an apparent impact on SST, as shown in the low SST in the tropical western IO accompanying strong cross-equatorial flow. The SST is highest in the equatorial central and eastern IO. Comparison between Fig. 1a, b indicates that the hindcast captures

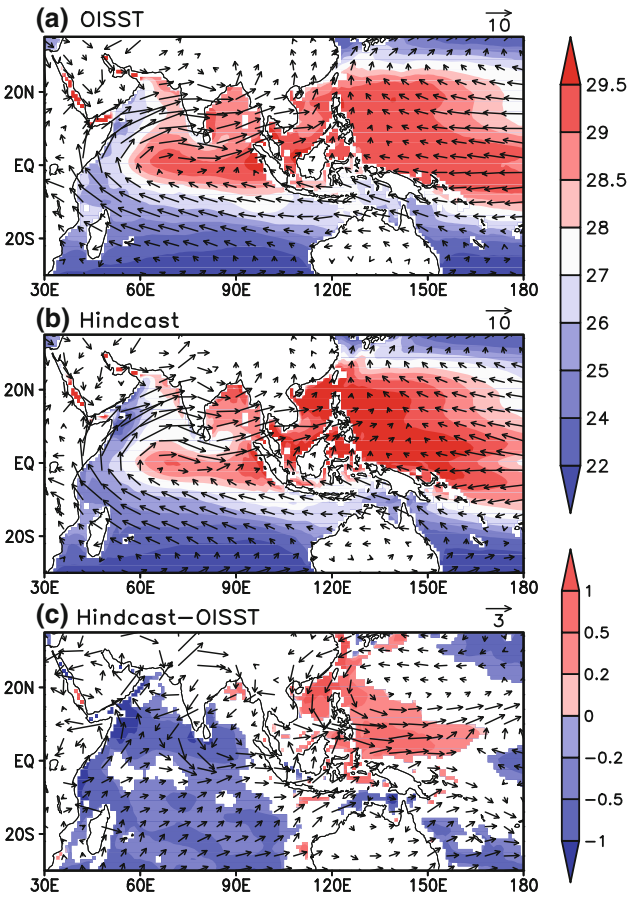

Fig. 1 Climatological JJA SST (°C; shading) and 850-hPa winds (m s^{-1}; vectors) for **a** observation, **b** 0-month lead hindcast, and **c** difference between **b** and **a**. Values below the 95 % confidence levels (t test) in **c** are omitted

the general features observed, including the monsoon flow and SST. However, the hindcast has a systematic cold bias in the tropical IO, while a warm bias appears in the WNP. The magnitude of cold bias in the northern IO is larger than that in the southern IO. It is also noted that the cold bias in the equatorial IO is smaller than that in the extra-equatorial regions, resulting in a meridional SST gradient that is favorable for enhancing convection over the equator. The feature is consistent with the excessive precipitation over the equatorial central and eastern IO (Jiang et al. 2013a).

To illustrate the possible causes of SST bias, we analyze the difference in total downward heat flux at the sea surface and ocean mixed layer depth between the 0-month lead hindcast and observation (Fig. 2). The predicted total downward heat flux is smaller than the observation in most regions. On the other hand, the CFSv2 predicted a deeper-than-observed mixed layer in most Indo-Pacific oceans, while a shallower-than-observed mixed layer is located in the WNP. The biases in total downward heat flux at sea surface and mixed layer depth contribute to the cold SST bias in the IO, except for part of the Bay of Bengal. In the WNP, the shallower-than-observed mixed layer contributes to the warm bias, while the heat flux bias favors a cold SST bias. Comparison between Figs. 1 and 2 indicates that the bias in mixed layer depth is similar to the bias in SST, indicating that the SST bias may be mainly ascribed to the bias in mixed layer depth. As shown in Fig. 1c, the

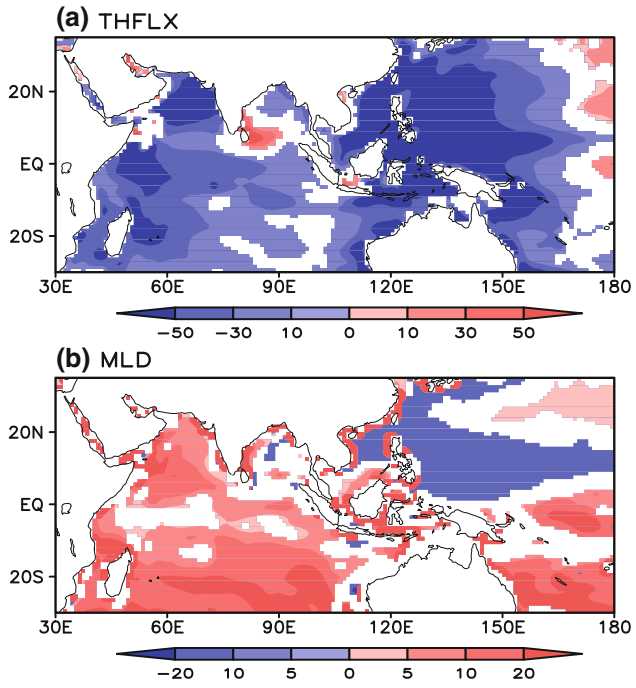

Fig. 2 Differences in **a** total downward heat flux at the sea surface and **b** ocean mixed layer depth between the 0-month lead hindcast and the CFS reanalysis from June to August. Values below the 95 % confidence levels (t test) are omitted

hindcast has a lower-tropospheric anomalous cyclone bias, which weakens the climatological winds at the western flank of the WPSH, contributing to the shallower-than-observed mixed layer and the resultant warm SST.

Figure 3 shows the first two leading modes and corresponding principal components (PCs) of an empirical orthogonal function (EOF) analysis of the temporal covariance matrix of JJA SST over the tropical IO for observation and 0-month lead hindcast. They account for 50 % (52 %) and 11 % (11 %) of the total variance of observation (0-month lead hindcast), respectively. The observed first mode features a basin-wide warming, while the second mode is characterized a dipole pattern, with warm SSTA in most central and western IO and cold SSTA in the western IO. It is also noted that the observed second mode has cold SSTA in the western Arabian Sea and the southwestern corner of the IO. The hindcast captures the uniform warming in the IO of the first mode, although it does not capture the warming center very well, with a pattern correlation coefficient of 0.31 between the hindcast and the observation. The dipole pattern of SST anomaly of the second mode is predicted by the hindcast, with a pattern correlation coefficient of 0.74 between the hindcast and observation. There is a positive trend in the principal component of the first mode (PC1), indicating an increase in tropical IO SST from 1983 to 2010. PC1 also exhibits a strong interannual variation. The hindcast captures the positive trend and interannual variation of the observed PC1, with a correlation coefficient of 0.93. The principal component of the second mode (PC2) does not show apparent long-term trend, but has a strong interannual variation. The hindcast also obtains the variation of the observed PC2, with a correlation coefficient of 0.60.

Figure 4a–c show the correlation of the observed Niño3.4 index at ENSO peak phase [from December D (0) to January–February JF (1), hereafter DJF (0/1)] with monthly Niño3.4 index, IOBW index, and IOD index from year (0) to year (1), respectively. Typically, ENSO first appears in May, reaches peak in winter, and terminates in the following summer. The hindcast captures the ENSO cycle very well. ENSO is associated with significant IOBW mode from December (0) to August (1), and significant IOD mode in autumn of the ENSO developing year. The hindcast captures the relationship of both IOBW and IOD with ENSO, but it shows higher skill for the IOBW. A longer-than-observed IOD event is also found in the hindcast. Generally, the hindcast predicts ENSO and its relationships with IOBW and IOD very well.

Figure 4d–f show the standard deviations of monthly Niño3.4 index, IOBW index, and IOD index. All ENSO, IOBW, and IOD indices exhibit apparent phase-lock features. ENSO is strong in winter but weak in summer; IOBW is strong in spring but weak in winter; and IOD is

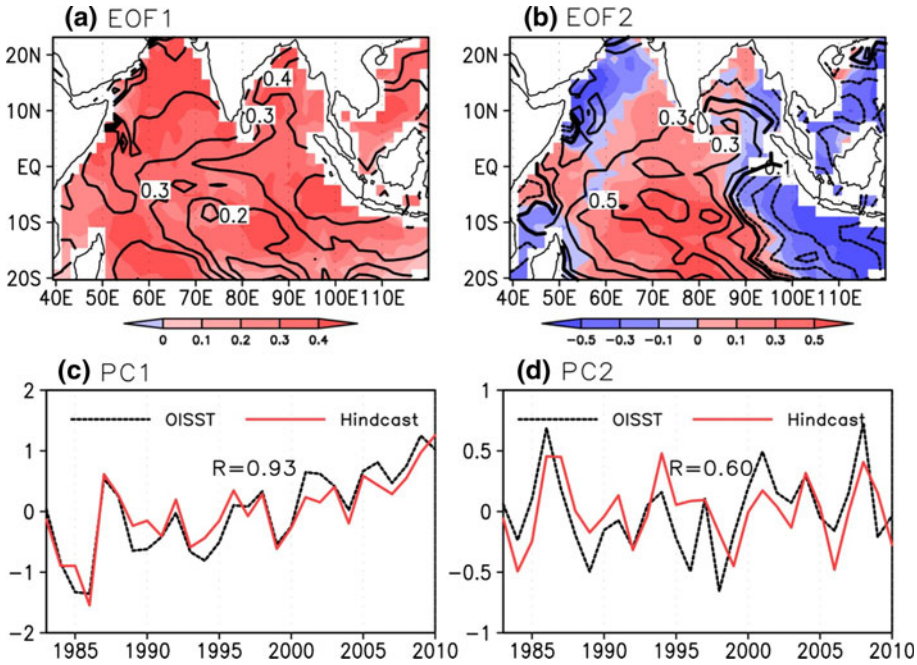

Fig. 3 **a** Spatial patterns and **c** principal components of the first mode of an EOF analysis of the temporal covariance matrix of JJA averaged SST from the OI SST (*shadings* for spatial pattern and *dash lines* for principal component) and from 0-month lead hindcast (*contours* for spatial pattern and *solid lines* for principal component). **b** and **d** are the same as **a** and **c**, but for the second mode

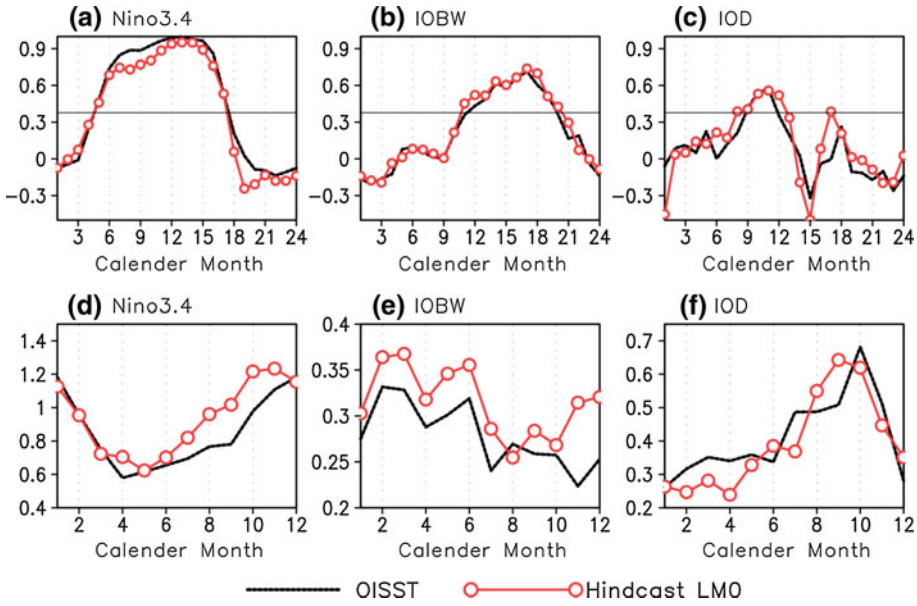

Fig. 4 Correlations of the observed DJF(0/1) Niño3.4 SST index with monthly **a** Niño3.4 SST index, **b** IOBW index, and **c** IOD index during the ENSO developing and decay years for the OI SST (*dash lines*) and 0-month lead hindcast (*solid lines* with *open circles*). Standard deviations of monthly **d** Niño3.4 SST index, **e** IOBW index, and **f** IOD index. *Straight solid lines* denote the 95 % confidence level

strong in autumn but weak in winter and spring. The hindcast realistically captures the magnitude of ENSO during its decaying phase, but depicts stronger-than-observed ENSO during the developing phase. The hindcast produces a stronger-than-observed IOBW, overestimates the IOD in August and September, and underestimates the IOD in spring.

3.2 Predictions as a function of lead time

The hindcast has a cold bias in the tropical IO and a warm bias in the WNP in summer for all time leads, but the magnitude of the bias in the tropical IO decreases with lead time. The feature is consistent with that the magnitude of predicted deeper-than-observed mixed layer and smaller-than-observed total downward heat flux in the tropical IO generally decreases as lead time increases (figures not shown). However, the predicted climatological summer monsoon circulation does not vary with lead time apparently (Jiang et al. 2013a). An EOF analysis of summer IO SST indicates that the hindcast captures the first IOBW mode for all time leads, especially the principal component (figures not shown). The dipole mode is also predicted for most time leads with an apparent spring predictability

barrier. It is interesting to mention that the variance explained by the first mode has a positive trend with lead time (figure not shown).

Figure 5 shows the correlation of the observed DJF(0/1) Niño3.4 SST index with monthly Niño3.4 SST, IOBW, and IOD indices respectively from year (0) to year(1) for different time leads. The prediction skill for monthly Niño3.4 index generally decreases with lead time. The predicted onset and decay of ENSO are later than the observed by about 1–2 months for the long leads. The ENSO-related IO warming is longer than observation when lead time is beyond 1 month, about one season earlier (later) than the observed onset (decay), respectively. The biases of 3- and 5-month lead predictions are larger than those of other time leads. A stronger-than-observed relationship between IOD and ENSO is found in most of the predictions from ENSO developing summer to the following summer. Overall, the hindcast has an apparent bias in simulating the response of IO SST to ENSO, although it shows a high skill in simulating ENSO cycle. Compared to the CFSv1 (see Fig. 3 in Chowdary et al. 2013), it seems that the ENSO and IOBW cycles are better represented by the CFSv2.

The predicted standard deviations of monthly Niño3.4, IOBW, and IOD indices of different time leads are presented in Fig. 6. The hindcast generally depicts a stronger-than-observed magnitude of ENSO, while it shows higher skill for the ENSO decaying phase than for the developing phase. The predicted magnitude of ENSO decreases during its developing phase as lead time increases, and even

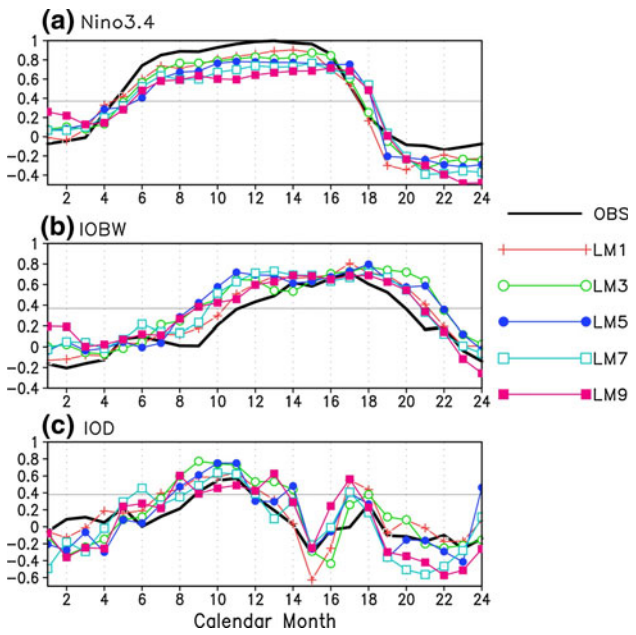

Fig. 5 Correlations of the observed DJF(0/1) Niño3.4 SST index with monthly **a** Niño3.4 SST index, **b** IOBW index, and **c** IOD index during the ENSO developing and decay years for the OI SST (*black solid lines*) and hindcast of different time leads (*color lines*)

weaker than observation for the predictions of lead time longer than 5 months. The hindcast generally simulates stronger-than-observed IOBW during winter and spring, which may be ascribed to the stronger-than-observed ENSO prediction. However, it produces weaker-than-observed IOBW from July to October and the magnitude decreases with increase in lead time. A weaker-than-observed IOD is found in the predictions of all time leads and the magnitude decreases strongly from 1-month lead to 3-month lead.

In summary, the hindcast captures the phase and magnitude of ENSO. It also depicts ENSO-related features of IOBW and IOD, but with stronger-than-observed links of IOBW and IOD to ENSO. The hindcast shows higher skill in simulating ENSO decay than ENSO development. The predicted summer IOBW and IOD are weaker than observations.

4 Relationship between IO SST and the western North Pacific anomalous anticyclone

4.1 Summer mean

As shown in Fig. 3c, the IOBW exhibits a strong warming trend. However, a close relationship between the IOBW and the WNPAC was found mostly in the ENSO decaying summer (Xie et al. 2009, 2010). Here, we thus focus on interannual variation of IOBW and its relationship with the WNPAC. Figure 7 shows the correlations of the observed detrended JJA IOBW index with JJA precipitation and SST, as well as the regressions of JJA 850-hPa winds on the observed detrended JJA IOBW. In observation, the IOBW is accompanied by easterlies over the northern IO, the WNPAC, and a cyclonic circulation over Northeast Asia. It is positively correlated with precipitation over the central Arabian Sea and northern Japan, but negatively correlated with precipitation over the Philippine Sea and the subtropical Northern Pacific. It has positive correlations with SST over most of the IO and the South China Sea, but negative correlation over the subtropical WNP (figure not shown), which is partially overlapped with the areas of negative correlation between IOBW and precipitation. The wind and precipitation patterns related to IOBW over the WNP and Japan are similar to the so-called Pacific-Japan pattern (Fig. 7a; Nitta 1987), which is an atmospheric manifestation of an air–sea coupled mode spanning the Indo-NWP warm pool, important for prediction of the WNP climate (Kosaka et al. 2013). The suppressed convection over the WNP plays an important role in driving the WNPAC (e.g. Xie et al. 2009; Wu et al. 2010; Wang et al. 2013). Compared to observation, the predicted 850-hPa winds related to the IOBW are weaker over the

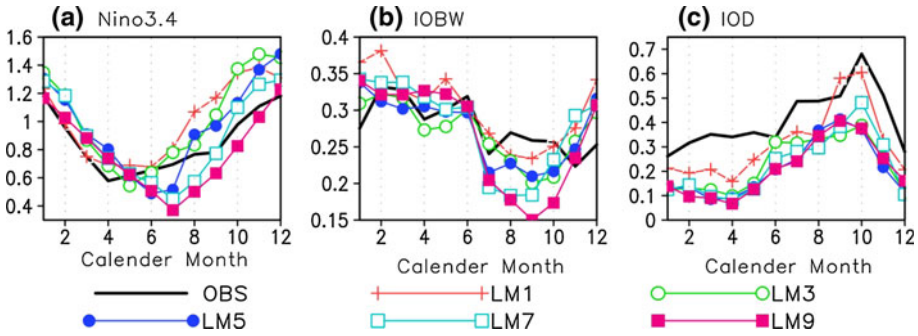

Fig. 6 Standard deviations of monthly **a** Niño3.4 SST index, **b** IOBW index, and **c** IOD index for the OI SST (*black solid lines*) and hindcast of different time leads (*color lines*)

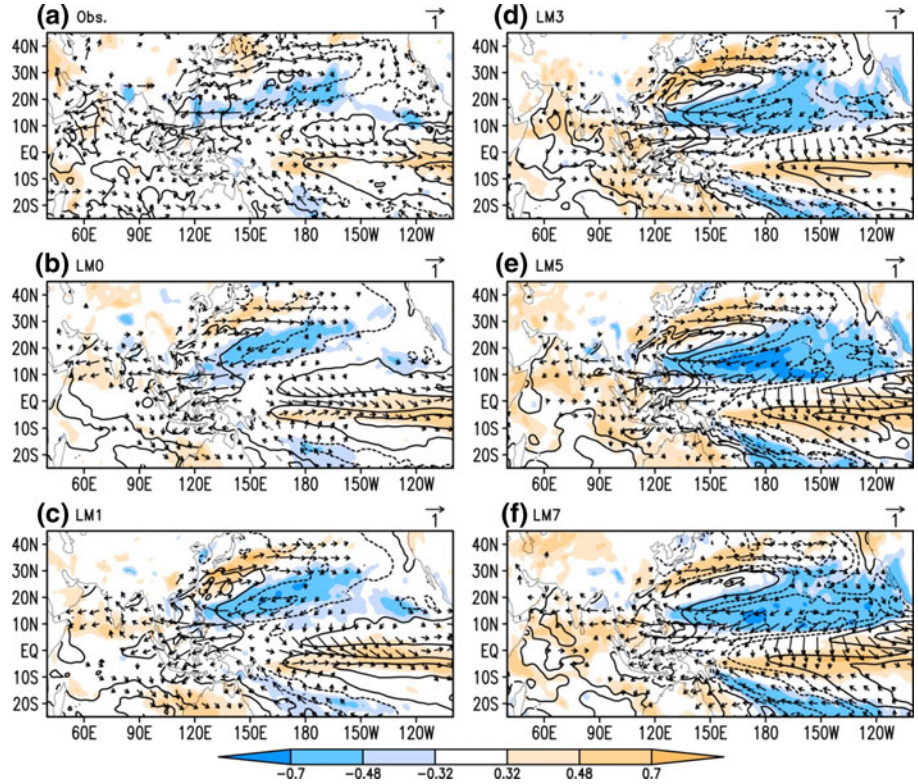

Fig. 7 Patterns of correlation of the observed detrended IOBW index with precipitation (*shading*) and SST (*contours*, with values of −0.7, −0.48, −0.2, 0.2, 0.48, and 0.7), respectively, and patterns of regression of 850-hPa winds (m s^{-1}; vectors) against the observed detrended IOBW index. (a) is for the observed precipitation and SST and **b–f** are for hindcast precipitation and SST of 0-month lead, 1-month lead, 3-month lead, 5-month lead, and 7-month lead, respectively. Correlation coefficients of 0.32 and 0.48 correspond to the 90 and 99 % confidence levels (t test), respectively. Wind vectors with speed smaller than 0.2 m s^{-1} are omitted

Indo-Pacific oceans. The hindcast captures the IOBW-related precipitation over the Arabian Sea and the subtropical WNP, but depicts a southward shift of heavy precipitation from northern Japan to south of Japan. The hindcast has an apparent bias: the relationships of the IOBW with winds, precipitation, and SST over the tropical Pacific strengthen with increase in lead time. This feature is also found between the Asia summer monsoon and the tropical Pacific climate in the CFSv2 (Jiang et al. 2013b).

The formation mechanisms of WNPAC may be different between long- and short-lead predictions. The WNPAC can be driven by the deficient precipitation and cold SSTA over the subtropical North Pacific for long time leads. Jiang et al. (2013a) reported that there might be a positive feedback among the WNPAC, deficient precipitation, and cold SST over the subtropical North Pacific during the ENSO decaying summer.

Figure 8 shows the correlations of the observed JJA IOD index with the observed and CFSv2 JJA precipitation, as well as the regressions of the observed and CFSv2 JJA 850-hPa winds on the observed JJA IOD index. In observation, the IOD is associated with the dipole patterns of SST and precipitation over the tropical IO, accompanied by lower-tropospheric easterlies. It is also associated with southwesterlies over southern India and is positively correlated with precipitation over Pakistan. The hindcast captures only the IOD-related features over the tropical IO for 0-month lead. It also simulates a stronger-than-observed ENSO-like pattern over the equatorial Pacific. The CFSv2's inability in predicting the climate impact of

IOD is consistent with that it cannot simulate the SST anomalies associated with the summer IOD index. Because the CFSv2 fails to predict summer IOD and its related features, we just discuss the features related to summer IOBW in the rest of the paper.

How does the IOBW affect the summer WNPAC? Xie et al. (2009, 2010) reported that the summer IOBW caused tropospheric temperature (TT) to increase by a moist-adiabatic adjustment, emanating a baroclinic Kelvin wave into the Pacific. This equatorial Kelvin wave induces northeasterly surface wind anomalies over the WNP, and the resultant divergence in the subtropics triggers suppressed convection and anomalous anticyclone. In addition, the IOBW strengthens the subtropical westerly jet stream, which enhances atmospheric convection over the Mei-yu rain band by advecting warm temperature from the Tibetan Plateau (Chowdary et al. 2010; Sampe and Xie 2010). The enhanced Mei-yu convection induces a surface wind divergence in the subtropics, resulting in depressed convection. Because the interannual variability of IOBW is

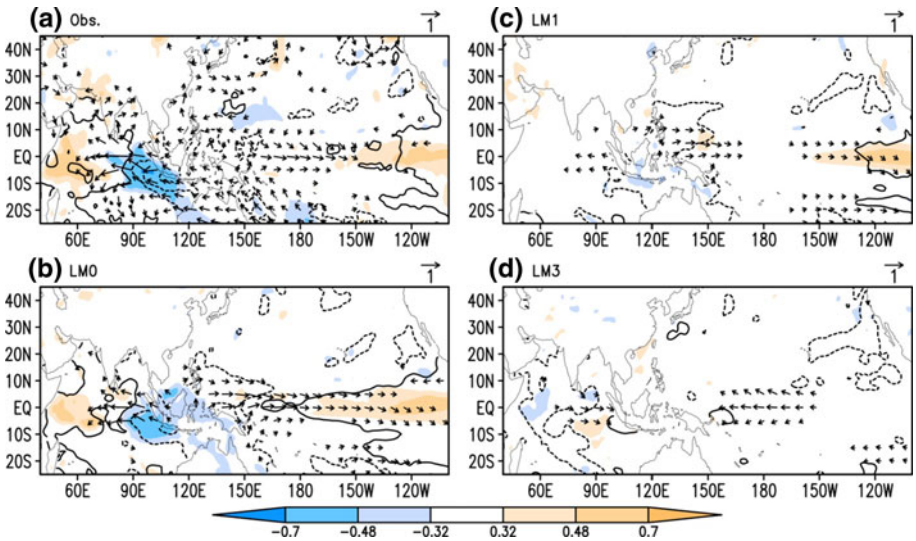

Fig. 8 Same as Fig. 7, but the observed detrended IOBW index is placed by the observed IOD index

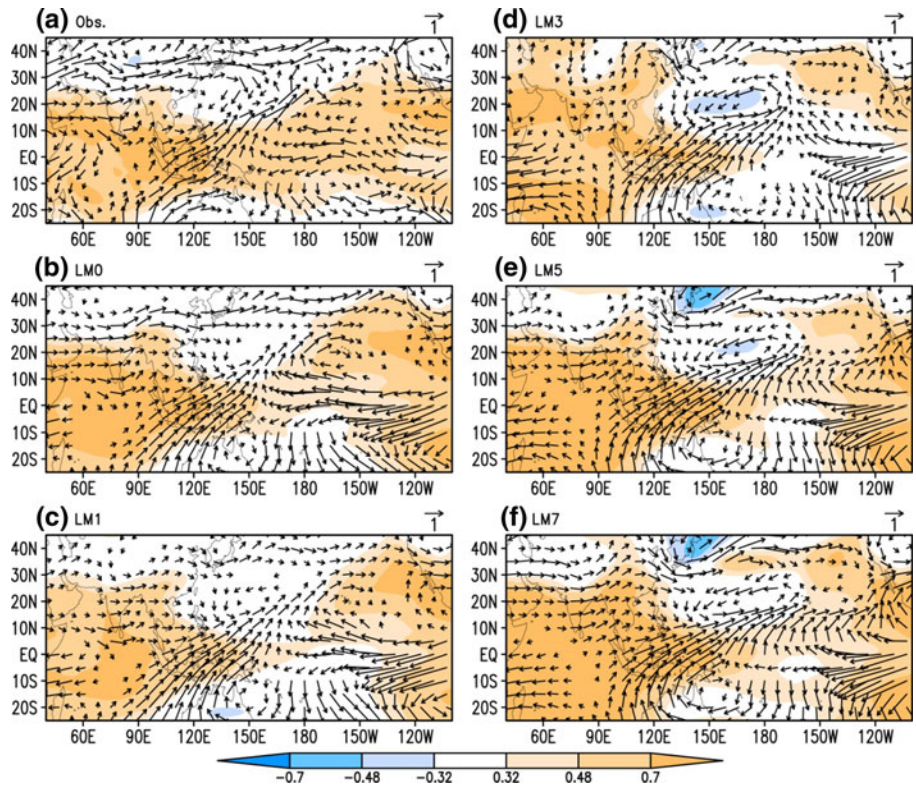

Fig. 9 Patterns of correlation between the observed DJF (0/1) Niño3.4 SST index and JJA (1) mean temperature of 500- and 300-hPa (shading) and regression of JJA (1) 200-hPa winds (m s^{-1}; vectors) against the observed DJF (0/1) Niño3.4 SST index for **a** the observed temperature and winds and hindcast temperature and winds of **b** 0-month lead, **c** 1-month lead, **d** 3-month lead, **e** 5-month lead, and **f** 7-month lead. Correlation coefficients of 0.32 and 0.48 are respectively corresponding to the 90 and 99 % confidence levels for t test. Wind vectors with speed smaller than 0.2 m s^{-1} are omitted

mostly as a response to ENSO, we now discuss the relationship between ENSO and the WANPAC more directly. We use the mean temperature of 500- and 300-hPa to represent TT based on the availability of hindcast data. Focusing on interannual variations, the linear trend of TT is extracted. It should be noted that the detrended IOBW-related patterns are similar to the patterns during ENSO decaying summer.

Figure 9 shows the ENSO-related TT and 200-hPa winds during ENSO decaying summer. As a response to the IOBW, TT anomalies show a Matsuno-Gill pattern (Matsuno 1966; Gill 1980). A warm Kelvin wave in TT propagates into the equatorial western Pacific, which causes lower-tropospheric northeasterlies on the northern flank of the Kelvin wave (Figs. 7a, 9a; Xie et al. 2009). The TT warming also strengthens the subtropical westerly jet stream over East Asia (Fig. 9a; Chowdary et al. 2010; Qu and Huang 2012). Corresponding to the WNPAC at the lower troposphere, there is a convergent wind pattern over the WNP at the upper troposphere. There are also two upper-tropospheric anticyclonic circulations over the central Pacific, located on each side of the equator symmetrically. The hindcast depicts the IOBW-related TT pattern for all time leads, but just captures the upper-tropospheric circulation for the short time leads. The IOBW-induced subtropical westerlies are only well captured by the 0-month lead prediction. The skills in predicting the IOBW-related TT patterns vary with lead time. The correlation between ENSO and the TT over the Indo-western Pacific for the long leads is higher than that observed. However, the IOBW-induced northeasterlies over the WNP are not evident in the predictions of lead time longer than 2 months. There is also a bias of upper-tropospheric cyclonic circulation in the predictions of lead time longer than 2 months, consistent with the bias of cold SSTA, deficient precipitation, and the lower-tropospheric anticyclonic circulation over the central subtropical Northern Pacific.

The above analysis indicates that the CFSv2 captures the IOBW-related WNPAC, but the maintenance mechanism for the WNPAC may be different. When lead time is shorter than two months, the IOBW is associated with the obvious TT anomalies over the Indo-western Pacific oceans and the resultant northeasterlies, which contribute to the maintenance of the WNPAC. However, the WNPAC may be mainly driven by the bias of depressed convection over the central subtropical North Pacific in the longer lead predictions. The CFSv2 fails to capture the possible impact of subtropical westerly jet stream over East Asia strengthened by the IOBW on the WNPAC.

4.2 Sub-seasonal variation

In addition to the IOBW, the local cold SST over the WNP may also be important for the summer WNPAC, especially in the early summer (Wu et al. 2010). Here, we further

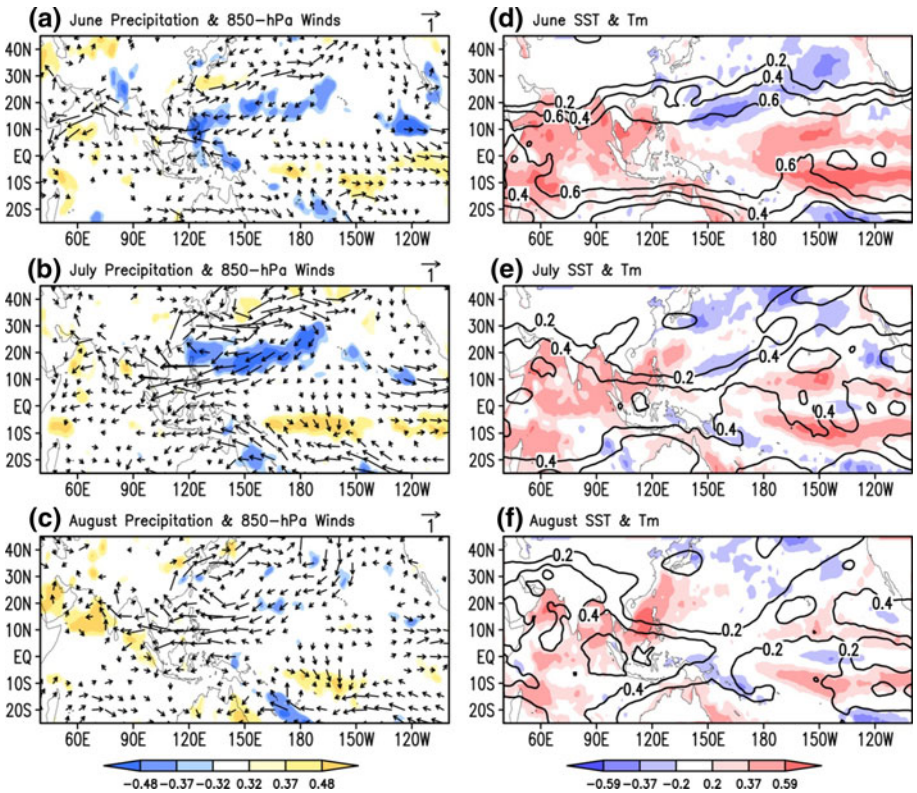

Fig. 10 **a** Observed patterns of correlation between DJF (0/1) Niño3.4 SST index and June (1) precipitation (*shading*), and regression of June (1) 850-hPa winds (m s^{-1}; *vectors*) against DJF (0/1) Niño3.4 SST index, **d** observed patterns of correlation of DJF(0/1) Niño3.4 SST index with June (1) SST and mean temperature of 500 and 300 hPa. **b** and **e**, **c** and **f** are same as **a** and **d**, but for July (1) and August (1), respectively. Wind vectors with speed smaller than 0.2 m s^{-1} are omitted

investigate the relative contribution of the local SST and the IOBW to the maintenance of WNPAC. We focus on sub-seasonal features.

Figure 10 shows the ENSO-related precipitation, SST, and 850-hPa winds in ENSO decaying June, July, and August, respectively. There is an obvious cold SSTA over the WNP in June, accompanied by deficient precipitation. The cold SSTA becomes weaker in July and almost disappears in August. The precipitation deficiency, however, intensifies from June to July. On the other hand, the WNPAC is weak in June, strengthens and moves northward in July, and reaches its peak in August covering the entire WNP with an even further northward shift of the ridgeline. The precipitation anomalies over East Asia are sensitive to the positions of the WNPAC: the excessive precipitation to the northern flank of the WNPAC moves northward from June to August. The WPSH also shows an apparent northward movement from June to July (figures not given). Thus, the sub-seasonal variation of the WNPAC may depend on the basic flow. It is interesting to note that the WNPAC is not associated with significant precipitation anomalies over the WNP in August, while ENSO has a significant positive correlation with precipitation over the western Arabian Peninsula, the central and eastern Arabian Sea, and the equatorial eastern IO. The correlation of ENSO with the IO SST decreases gradually from June to August. The ENSO-related TT in June is zonally oriented, but it shows a warm Kelvin wave propagating into the equatorial western Pacific in July and August. Thus, it seems that the IOBW may not affect the WNPAC in June by the way proposed by Xie et al. (2009).

Figure 11 shows the ENSO-related SST, precipitation, and 850-hPa winds in June predicted by the CFSv2 for different time leads. Comparisons among Figs. 10a, d, and 11 indicate that the 0-month lead hindcast captures the major features related to ENSO, although it overestimates the response of SST and 850-hPa winds to ENSO. The deficient precipitation is overlapped with the cold SSTA, accompanied by the WNPAC to the northwest. The predicted SST, precipitation, and 850-hPa winds over the WNP do not show apparent differences as lead time increases. However, the correlations of ENSO with SST and precipitation over the tropical central and eastern Pacific strengthen with increase in lead time especially when lead time is longer than 3 months, accompanied by the bias of 850-hPa northerlies over the equatorial central and eastern Pacific. The correlation between ENSO and precipitation over the tropical IO is also overestimated when lead time is longer than 3 months. While the CFSv2 captures the ENSO-related zonally oriented TT for most time leads, it has a bias in predicting the warm Kelvin wave propagating into the equatorial western Pacific in the 1- and 3-month lead predictions (figures not shown).

ENSO-related features in July predicted by the CFSv2 for different time leads are demonstrated in Fig. 12. The 0-month lead hindcast simulates a weaker-than-observed

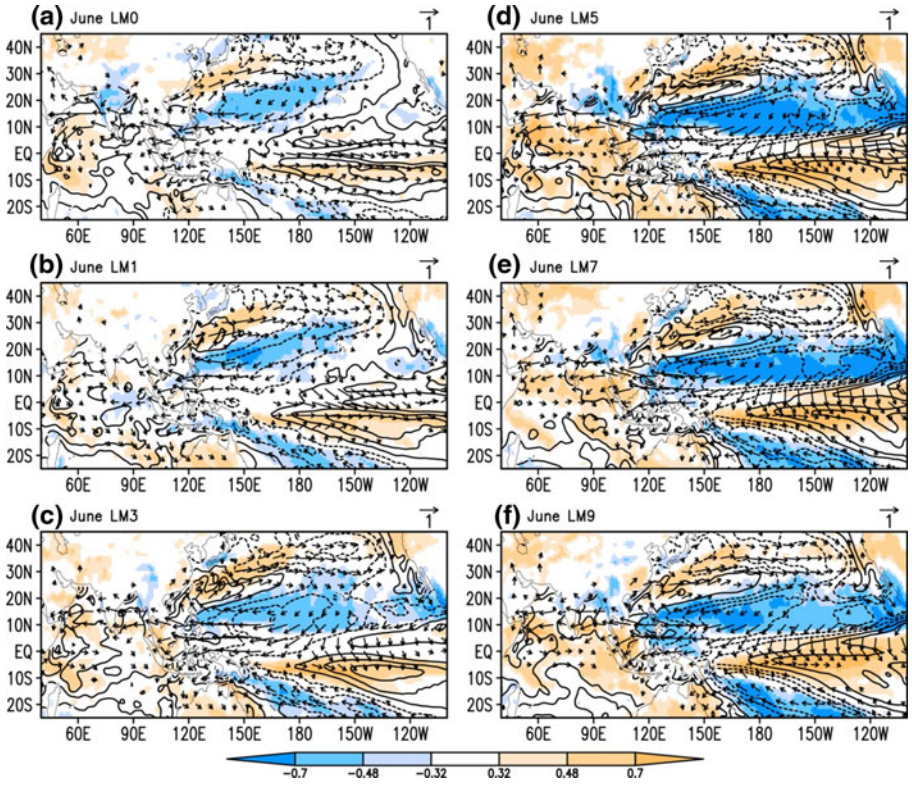

Fig. 11 Patterns of correlation of the observed DJF (0/1) Niño3.4 SST index with June (1) precipitation (*shading*) and SST (*contours*; values of contours are −0.7, −0.48, −0.2, 0.2, 0.48, and 0.7), and patterns of regression of June (1) 850-hPa winds (m s^{-1}; *vectors*) against DJF (0/1) Niño3.4 SST index. **a**–**f** are for hindcast of 0-month lead, 1-month lead, 3-month lead, 5-month lead, 7-month lead, and 9-month lead, respectively. Correlation coefficient of 0.32 and 0.48 are respectively corresponding to the 90 and 99 % confidence levels for t test. Wind vectors with speed smaller than 0.2 m s^{-1} are omitted

WNPAC and captures the correlation between ENSO and precipitation over the WNP especially the northern Philippine Sea. It also depicts a stronger-than-observed negative correlation between ENSO and SST over the WNP. However, the correlations of ENSO with precipitation and SST over the WNP strengthen in the 1- and 3-month lead predictions, accompanied by a realistic WNPAC. When lead time is longer than 3 months, the hindcast shows stronger-than-observed correlation between ENSO and the climate over the tropical Pacific. The northern edge of ENSO-related precipitation and SST over the WNP also moves southward, resulting in a weak WNPAC and southward shift of its northern edge from 5-month lead prediction to 7-month lead prediction. The CFSv2 predicts the observed warm Kelvin wave propagating into the equatorial western Pacific for all time leads (figures not shown). However, the related northeasterlies are just well captured by the 1- and 3-month lead predictions, consistent with the well-predicted precipitation and anticyclonic circulation over the WNP. It is also noted that the deficient precipitation is mostly overlapped with the cold SSTA over the WNP except the western Philippine Sea when northeasterlies prevail to its south.

Figure 13 shows ENSO-related SST, precipitation, 850-hPa winds in August predicted by the CFSv2 for different time leads. A weaker-than-observed WNPAC but stronger-than-observed correlations of ENSO with precipitation and SST over WNP are found in the predictions from 0-month lead to 3-month lead. The stronger-than-observed correlation between ENSO and tropical Pacific climate is also found in the long lead predictions for August. The patterns of correlation between ENSO and precipitation over the IO are captured by the CFSv2, but the correlation between ENSO and precipitation over the tropical eastern IO also strengthens with increase in lead time. Although the observed WNPAC in August is not accompanied by significant precipitation anomalies over the WNP, the magnitude of WNPAC depends on the magnitude of ENSO-related precipitation deficiency over the WNP in the hindcast. The observed warm Kelvin wave propagating into the equatorial western Pacific in August can be predicted for all time leads (figures not shown). However, the northeasterlies associated with the warm Kelvin wave are only captured by the CFSv2 when lead time is less than 5 months, which favors precipitation deficiency over the southern Philippine Sea and equatorial western Pacific, where no negative correlation between ENSO and SST is found. The inability of long lead predictions in depicting the northeasterlies over the tropical WNP may be ascribed to the bias of deficient precipitation over the central North Pacific, which induces an anticyclonic circulation that causes southeasterlies over the tropical WNP, weakening the northeasterlies caused by the warm Kelvin wave.

Comparison among Figs. 10, 11, 12 and 13 indicates that the hindcast shows higher skill in depicting the climate

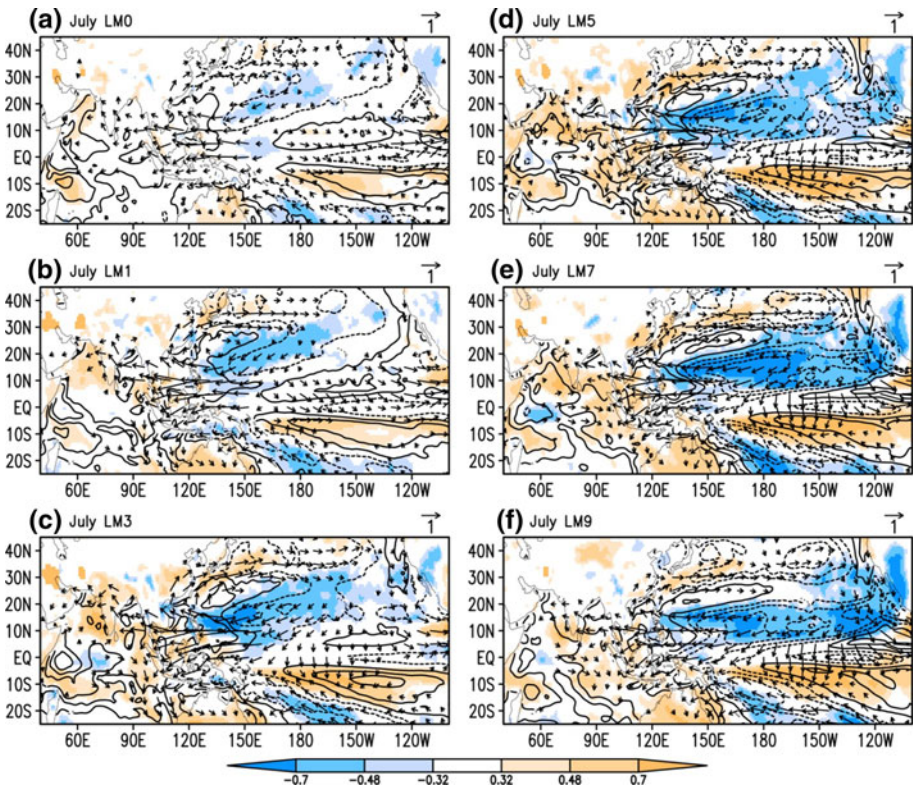

Fig. 12 Same as Fig. 11, but for July

anomalies over the WNP in June than in July and August. The CFSv2 tends to have weaker-than-observed precipitation anomalies and anticyclonic circulations over the WNP in July and August for the 0-month lead prediction compared to other time leads, in which deficient precipitation is overlapped by cold SSTA. The 1- and 3-month lead predictions capture the IOBW-excited warm Kelvin wave propagating into the equatorial western Pacific and the resultant northesterlies over the tropical WNP, which favor suppressed convection over the tropical WNP and resultant WNPAC. There are apparent biases of cold SSTA and deficient precipitation over the central and eastern subtropical North Pacific, which contribute to the maintenance of WNPAC in long lead predictions. The CFSv2 captures the northward advance of the WNPAC from June to August. The CFSv2 also simulates stronger-than-observed correlation between ENSO and precipitation over the IO in long lead predictions.

5 Summary and discussion

The NCEP CFSv2, which became operational in March 2011, provides important source of information about the seasonal climate prediction over many regions of the world. In this study, we have provided a comprehensive assessment of the prediction of the tropical IO SST. We have also investigated the impact of IO SST on Indo-western Pacific summer climate in both observation and CFSv2 hindcast, focusing on the relative contribution of local SST and remote forcing to the anomalous anticyclonic circulation over the WNP, which plays an important role in the variability of East Asian climate.

The CFSv2 captures the spatial pattern of tropical IO SST in summer, but produces a systematic cold bias in the tropical IO, which may be ascribed to the predicted deeper-than-observed mixed layer and smaller-than-observed total downward heat flux in the tropical IO. The first two leading EOF modes of tropical IO SST are well predicted by the CFSv2. The model captures the phase and magnitude of ENSO, while predicts stronger-than-observed correlations of ENSO with IOBW and IOD. It also underestimates the magnitude of IOD and summer IOBW.

The CFSv2 captures the interannual variation of summer IOBW and related climate anomalies over the IO-Pacific oceans especially the WNPAC. However, it fails to predict the possible climate impact of IOD. The model captures the impact of summer IOBW on WNPAC by the way proposed by Xie et al. (2009), while it fails to capture the possible impact of the subtropical westerly jet over East Asia strengthened by IOBW on the WNPAC (Chowdary et al. 2010; Sampe and Xie 2010). The CFSv2 has a strong cold bias in the subtropical central and eastern North Pacific for the prediction of long time leads, which causes deficient

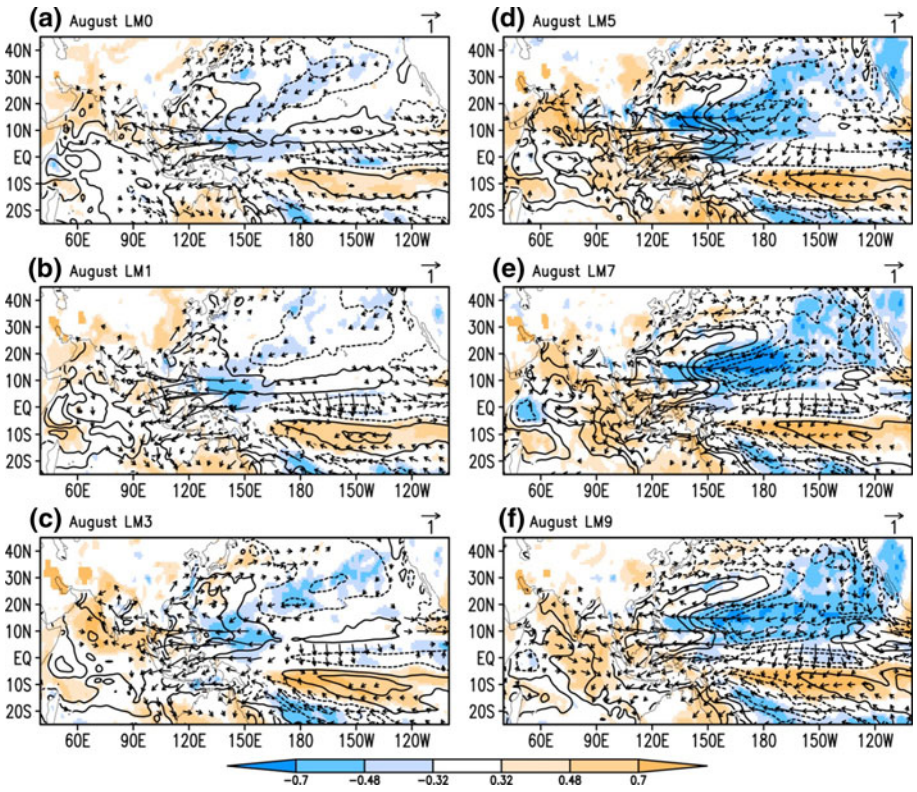

Fig. 13 Same as Fig. 11, but for August

precipitation and the resultant anticyclonic circulation over the WNP. This bias may impede that the CFSv2 simulates the impact of IOBW on the WNPAC by changing the feedback between convection and atmospheric circulation over the subtropical WNP. Besides ENSO and the IO SST, other factors such as the North Atlantic Oscillation and the Tibetan Plateau snow cover can also affect the variations of the WPSH (Wu et al. 2009, 2012a, b). Thus, the CFSv2's skill in predicting the WNPAC may not solely depend on the ways explored in this study.

During the ENSO decaying phase, the climate anomalies over the WNP exhibit apparent sub-seasonal variations. The ENSO-related TT in June is zonally oriented, while it shows a warm Kelvin wave propagating into the equatorial western Pacific in July and August. It seems that the WNPAC in June is mainly forced by the local cold SSTA, consistent with the AMIP-type simulation of Wu et al. (2010). The CFSv2 captures the major features of the sub-seasonal variation of ENSO-related climate anomalies over the WNP. It shows high skill in predicting the WNPAC in June, because the deficient precipitation predicted is mainly overlapped with the cold SSTA over the WNP. The mechanisms for the maintenance of WNPAC in July and August in the hindcast vary with lead time. Only the predictions of 1- and 3-month leads capture the impact of IOBW on the WNPAC, resulting in decent predictions of the WNPAC.

The CFSv2 shows low skill in predicting the IOD, which is a dynamically coupled atmosphere–ocean mode and exhibits a strong seasonality (e.g. Li et al. 2003), and its possible climate impact. The low skill in predicting the IOD is not limited to CFSv2 though. Shi et al. (2012) reported that most operational climate prediction systems cannot predict the mature IOD prior to about May. The low predictability of IOD may be attributed to the seasonality of IOD (Li et al. 2003), the mean state bias in the IO (Fischer et al. 2005), and the bias in predicting the link of IOD to ENSO (Shi et al. 2012). This study shows that the CFSv2 has an apparent cold SST bias in the IO and it overestimates the response of the IO SST to ENSO. Not only the SST but also the atmospheric circulations over the Indo-Pacific oceans show an exaggerated link to ENSO (Jiang et al. 2013a, b). In addition, the CFSv2 has bias in simulating the climatological features of the South Asian summer monsoon (Jiang et al. 2013a, b). All these factors may lead to the failure of IOD prediction by the CFSv2. Further studies on this issue are undoubtedly necessary.

Acknowledgments The authors thank the two anonymous reviewers for their constructive comments, which improve the overall quality of the paper. This study was jointly supported by the National Natural Science Foundation of China (Grant 41105061), the National Basic Research Program of China (Grant 2012CB417202), and the Basic Research and Operation Program of the Institute of Plateau Meteorology, CMA (Grant BROP201215, BROP201318), and the Sun Yat-sen University "985 Project" Phase 3. Xingwen Jiang, who was partially supported by US National Oceanic and Atmospheric Administration and China Meteorological Administration Bilateral Program, thanks NOAA's Climate Prediction Center for hosting his visit while this study was conducted.

References

Ashok K, Guan Z, Yamagata T (2001) Impact of the Indian Ocean dipole on the relationship between the Indian monsoon rainfall and ENSO. Geophys Res Lett 28:4499–4502. doi:10.1029/2001GL013294

Behera SK, Luo JJ, Masson S et al (2005) Paramount Impact of the Indian Ocean Dipole on the East African short rains: a CGCM study. J Clim 18:4514–4530

Chang CP, Zhang YS, Li T (2000) Interannual and interdecadal variations of the East Asian summer monsoon and tropical Pacific SSTs. Part I: roles of the subtropical ridge. J Clim 13:4310–4325

Chowdary JS, Xie SP, Lee JY, Kosaka Y, Wang B (2010) Predictability of summer northwest Pacific climate in 11 coupled model hindcasts: local and remote forcing. J Geophys Res 115:D22121. doi:10.1029/2010JD014595

Chowdary JS, Xie SP, Luo JJ et al (2011) Predictability of Northwest Pacific climate during summer and the role of the tropical Indian Ocean. Clim Dyn 36:607–621. doi:10.1007/s00382-009-0686-5

Chowdary JS, Chaudhari HS, Gnanaseelan C, Parekh A, Suryachandra Rao A, Sreenivas P, Pokharel S, Singh P (2013) Summer monsoon circulation and precipitation over the tropical Indian Ocean during ENSO in the NCEP climate forecast system. Clim Dyn. doi:10.1007/s00382-013-1826-5

Ding RQ, Ha K-J, Li JP (2010) Interdecadal shift in the relationship between the East Asian summer monsoon and the tropical Indian Ocean. Clim Dyn 34:1059–1071

Fasullo J, Webster PJ (2002) Hydrological signatures relating the Asian summer monsoon and ENSO. J Clim 15:3082–3095

Fischer AS, Terray P, Guilyardi E, Gualdi S, Delecluse P (2005) Two independent triggers for the Indian Ocean dipole/zonal mode in a coupled GCM. J Clim 18:3428–3449

Gill AE (1980) Some simple solutions for heat-induced tropical circulation. Q J R Meteorol Soc 106:447–462. doi:10.1002/qj.49710644905

Huang G, Hu K, Xie SP (2010) Strengthening of tropical Indian Ocean teleconnection to the Northwest Pacific since the mid-1970s: an atmospheric GCM study. J Clim 23:5294–5304

Jiang XW, Li JP (2011) Influence of the annual cycle of sea surface temperature on the monsoon onset. J Geophys Res 116:D10105. doi:10.1029/2010JD015236

Jiang XW, Yang S, Li Y, Kumar A, Liu X, Zuo Z, Jha B (2013a) Seasonal-to-interannual prediction of the Asian summer monsoon in the NCEP Climate Forecast System Version 2. J Clim 26:3708–3727

Jiang XW, Yang S, Li Y, Kumar A, Wang W, Gao Z (2013b) Dynamical prediction of the East Asian winter monsoon by the NCEP climate forecast system. J Geophys Res 118:1312–1328. doi:10.1002/jgrd.50193

Kosaka K, Xie SP, Lau NC, Vecchi GA (2013) Origin of seasonal predictability for summer climate over the Northwestern Pacific. Proc Natl Acad Sci USA 110:7574–7579

Kripalani RH, Oh JH, Chaudhari HS (2010) Delayed influence of the Indian Ocean Dipole mode on the East Asia–West Pacific monsoon: possible mechanism. Int J Climatol 30:197–209. doi:10.1002/joc.1890

Kug J-S, Kang I-S (2006) Interactive feedback between ENSO and the Indian Ocean. J Clim 19:1784–1801
Lau NG, Wang B (2006) Interaction between the Asian Monsoon and El Nino/Southern Oscillation. The Asian Monsoon, Wang B (ed), Praxis, pp 479–512
Li JP, Ding RQ (2012) Temporal–spatial distribution of the predictability limit of monthly sea surface temperature in the global oceans. Int J Climatol. doi:10.1002/joc.3562
Li T, Wang B (2005) A review on the western North Pacific monsoon: synoptic-to-interannual variabilities. Terr Atmos Ocean Sci 16:285–314
Li T, Wang B, Chang CP, Zhang Y (2003) A theory for the Indian Ocean dipole-zonal mode. J Atmos Sci 60:2119–2135
Li JP, Wu ZW, Jiang ZH, He JH (2010) Can global warming strengthen the East Asian summer monsoon? J Clim 23: 6696–6705
Matsuno T (1966) Quasi-geostrophic motions in the equatorial area. J Meteorol Soc Jpn 44:25–43
Nitta T (1987) Convective activities in the tropical western Pacific and their impact on the Northern Hemisphere summer circulation. J Meteorol Soc Jpn 65:373–390
Pokhrel S, Chaudhari H, Saha S et al (2012) ENSO, IOD and Indian summer monsoon in NCEP climate forecast system. Clim Dyn 39:2143–2165
Qu X, Huang G (2012) Impacts of tropical Indian Ocean SST on the meridional displacement of East Asian jet in boreal summer. Int J Climatol 32(13):2073–2080
Reynolds RW, Smith TM, Liu C et al (2007) Daily high-resolution blended analyses for sea surface temperature. J Clim 20: 5473–5496
Saha S et al (2006) The NCEP climate forecast system. J Clim 19: 3483–3517
Saha S et al (2010) The NCEP climate forecast system reanalysis. Bull Am Meteorol Soc 91:1015–1057
Saji NH, Yamagata T (2003) Possible impacts of Indian Ocean dipole mode events on global climate. Clim Res 25(2):151–169
Saji NH, Goswami BN, Vinayachandran PN, Yamagata T (1999) A dipole mode in the tropical Indian Ocean. Nature 401:360–363
Sampe T, Xie SP (2010) Large-scale dynamics of the Meiyu-Baiu rainband: environmental forcing by the westerly jet. J Clim 23:113–134
Shi L, Hendon H, Alves O et al (2012) How predictable is the Indian Ocean dipole? Mon Weather Rev 140:3867–3884
Shukla J, Paolina DA (1983) The southern oscillation and long range forecasting of the summer monsoon rainfall over India. Mon Weather Rev 111:1830–1837
Wang B, Wu R, Fu X (2000) Pacific-East Asia teleconnection: how does ENSO affect East Asian climate? J Clim 13:1517–1536
Wang B, Wu R, Li T (2003) Atmosphere-Warm Ocean interaction and its impact on Asian-Australian Monsoon variation. J Clim 16:1195–1211
Wang B, Ding QH, Fu XH, Kang IS, Jin K, Shukla J, Doblas-Reyes F (2005) Fundamental challenge in simulation and prediction of summer monsoon rainfall. Geophys Res Lett 32:L15711
Wang W, Xie P, Yoo SH, Xue Y, Kumar A, Wu X (2010) An assessment of the surface climate in the NCEP climate forecast system reanalysis. Clim Dyn 37:1601–1620
Wang B, Xiang B, Lee JY (2013) Subtropical High predictability establishes a promising way for monsoon and tropical storm predictions. Proc Natl Acad Sci 110:2718–2722
Webster PJ, Magana VO, Palmer TN, Shukla J, Tomas RA, Yanai M, Yasunari T (1998) Monsoons: processes, predictability, and the prospects for prediction. J Geophys Res 103:14451–14510
Webster PJ, Moore A, Loschnigg J, Leban M (1999) Coupled ocean–atmosphere dynamics in the Indian Ocean during 1997–98. Nature 40:356–360
Wu R, Kirtman BP (2004a) Impacts of Indian Ocean on the Indian monsoon-ENSO relationship. J Clim 17:3037–3054
Wu R, Kirtman BP (2004b) Understanding the impacts of the Indian Ocean on ENSO variability in a coupled GCM. J Clim 17: 4019–4031
Wu Z, Wang B, Li J, Jin F (2009) An empirical seasonal prediction model of the East Asian summer monsoon using ENSO and NAO. J Geophys Res 114:D18120. doi:10.1029/2009JD011733
Wu B, Li T, Zhou T (2010) Relative contributions of the Indian Ocean and local SST anomalies to the maintenance of the western North Pacific anomalous anticyclone during El Nino decaying summer. J Clim 23:2974–2986
Wu Z, Li J, Jiang Z, Ma T (2012a) Modulation of the Tibetan Plateau snow cover on the ENSO teleconnections: from the East Asian summer monsoon perspective. J Clim 25:2481–2489
Wu Z, Jiang Z, Li J, Zhong S, Wang L (2012b) Possible association of the western Tibetan Plateau snow cover with the decadal to interdecadal variations of northern China heatwave frequency. Clim Dyn 39:2393–2402. doi:10.1007/s00382-012-1439-4
Xie P, Arkin PA (1997) Global precipitation: a 17-year monthly analysis based on gauge observations, satellite estimates, and numerical model outputs. Bull Am Meteorol Soc 78:2539–2558
Xie SP, Hu K, Hafner J, Tokinaga H, Du Y, Huang G, Sampe T (2009) Indian Ocean capacitor effect on Indo-western Pacific climate during the summer following El Niño. J Clim 22: 730–747
Xie SP, Du Y, Huang G et al (2010) Decadal shift in El Nino influences on Indo-western Pacific and East Asian climate in the 1970s. J Clim 23:3352–3368
Yang S, Zhang Z, Kousky VE, Higgins RW, Yoo SH, Liang J, Fan Y (2008) Simulations and seasonal prediction of the Asian summer monsoon in the NCEP Climate Forecast System. J Clim 21:3755–3775
Yoo SH, Yang S, Ho CH (2006) Variability of the Indian Ocean sea surface temperature and its impacts on Asian-Australian monsoon climate. J Geophys Res 111:D03108
Yoo SH, Fasullo J, Yang S, Ho CH (2010) On the relationship between Indian Ocean sea surface temperature and the transition from El Nino to La Nina. J Geophys Res 115:D15114. doi:10.1029/2009JD012978
Yu J-Y, Lau KM (2004) Contrasting Indian Ocean SST variability with and without ENSO influence: a coupled atmosphere-ocean GCM study. Meteorol Atmos Phys. doi:10.1007/s00703-004-0094-7
Yu J-Y, Mechoso CR, McWilliams JC, Arakawa A (2002) Impacts of the Indian Ocean on the ENSO cycle. Geophys Res Lett 29:1204. doi:10.1029/2001GL014098
Yuan X, Wood EF, Luo L, Pan M (2011) A first look at Climate Forecast System version 2 (CFSv2) for hydrological seasonal prediction. Geophys Res Lett 38:L13402
Yuan Y, Yang S, Zhang Z (2012) Different evolutions of the Philippine Sea anticyclone between eastern and central Pacific El Niño: possible effect of Indian Ocean SST. J Clim 25:7867–7883
Zheng XT, Xie SP, Liu Q (2011) Response of the Indian Ocean basin mode and its capacitor effect to global warming. J Clim 24: 6146–6164